IOPscience iopscience.iop.org

Home Search Collections Journals About Contact us My IOPscience

Flash imprint lithography using a mask aligner: a method for printing nanostructures in photosensitive hydrogels

This article has been downloaded from IOPscience. Please scroll down to see the full text article.

2008 Nanotechnology 19 215303

(http://iopscience.iop.org/0957-4484/19/21/215303)

View the table of contents for this issue, or go to the journal homepage for more

Download details:
IP Address: 128.54.34.2
The article was downloaded on 12/09/2013 at 22:28

Please note that terms and conditions apply.

Nanotechnology **19** (2008) 215303 (13pp) doi:10.1088/0957-4484/19/21/215303

Flash imprint lithography using a mask aligner: a method for printing nanostructures in photosensitive hydrogels

David Y Fozdar[1,2], Wande Zhang[1,2], Marylene Palard[2], Charles W Patrick Jr[3] and Shaochen Chen[1,2,4]

[1] Department of Mechanical Engineering, Center for Nano Molecular Science and Technology (CNM), The University of Texas at Austin, 1 University Station, C2200 & A5500 (CNM), Austin, Texas 78712, USA
[2] Microelectronics Research Center, The University of Texas at Austin, 10100 Burnett Road, Bldg 160, Austin, Texas 78758, USA
[3] Department of Biomedical Engineering, The University of Texas M D Anderson Cancer Center, 1515 Holcombe Boulevard, Unit 193, Houston, Texas 77030, USA

E-mail: scchen@mail.utexas.edu

Received 5 November 2007, in final form 21 March 2008
Published 21 April 2008
Online at stacks.iop.org/Nano/19/215303

Abstract
In this paper, we report a general method for imprinting nanometer-scale features in low-viscosity photosensitive hydrogels using conventional optical mask aligner technology. We call this method flash imprint lithography using a mask aligner (FILM). The FILM process makes it possible to fabricate nanometer-scale features in ultraviolet (UV)-curable hydrogels quickly, inexpensively and reproducibly. We believe that the FILM process will be useful in many areas of research but is particularly applicable to tissue engineering. Accordingly, we demonstrate the FILM process by imprinting dense arrays of nanostructures in polyethylene glycol dimethacrylate (PEGDMA), a material commonly utilized as a substrate in micro-and nanoscale tissue scaffolds; finite element modeling and contact angle analysis are employed to characterize pattern transfer of low-viscosity polymers (e.g. PEGDMA) in the FILM process.

(Some figures in this article are in colour only in the electronic version)

1. Introduction

Optical lithography is the most widely utilized process for manufacturing integrated circuits, MEMS and microfluidic devices, and related technologies. Optical lithography prints microscale features in optically sensitive polymers accurately, precisely and with high throughput. A few groups have reported using optical lithography to pattern microscale features in UV-curable PEG hydrogels using conventional photomasks [1, 2]. Unfortunately, because of the desire to pattern nanoscale features in many new applications, particularly in advanced tissue scaffold fabrication, optical lithography is insufficient because of its inability to transfer geometrical information beyond the diffraction limit. While efforts are being made to try to circumvent this limit, it is important to note that solutions to the diffraction problem have to be amenable to the reproducible and high-throughput requirements inextricably linked to industrial manufacturing and many applications in research. Other widely utilized nanofabrication technologies, like focused-ion-beam writing (FIB) and electron-beam lithography (EBL), have been able to directly write features down to a few nanometers; however, these serial direct-write techniques are too time-consuming for production on even moderate scales. The future of nanoscale-based engineering will depend largely on the development of innovative nanofabrication processes and technologies that can, accurately and precisely, produce nanometer-scale features with reasonably high throughput. One such innovative fabrication process, nanoimprint lithography (NIL), introduced by Chou *et al* [3], is the process of embossing features from a mechanically hard mold into thermoplastic materials heated above their glass transition temperature. Chou *et al* [3] were able to imprint 25 nm holes from a silicon mold

[4] Author to whom any correspondence should be addressed.

 © 2008 IOP Publishing Ltd Printed in the UK

into polymethylmethacrylate (PMMA). The silicon mold was patterned using EBL and etched using reactive-ion-etching (RIE). A more recently demonstrated process, step-and-flash imprint lithography (S-FIL), introduced by Colburn *et al* [4], is the process of imprinting the features of a transparent mold (e.g. quartz) into a photosensitive polymer. The polymer is a low-viscosity liquid that cures upon exposure to ultraviolet (UV) light emanating through the mold. The S-FIL process utilizes a transfer material layer and the nanopatterned UV-curable polymer as etch barriers for the ultimate patterning of the substrate (e.g. silicon) by RIE [4]. The enabling step-and-flash process opened the door to a new genre of imprinting techniques by adapting conventional NIL for use with UV-curable polymers rather than just thermoplastic materials.

Although the S-FIL process has been developed markedly since its inception and, indeed, is a very promising technology, it requires the use of unconventional dedicated nanoimprinting tools (e.g. IMPRIO 55, 100 and 250 by Molecular Imprints, Austin, TX). Such dedicated imprinting tools are typically unavailable in most cleanrooms and require extremely costly imprinting templates and ad hoc drop dispensers to support different UV-curable materials. Other promising variations of UV-based imprinting, like UV nanoimprint lithography (UV-NIL), have been demonstrated; however, they either continue to utilize specialized nanoimprinting tools like the S-FIL process or are alternatives that lack the control and automation intrinsic to using nanoimprinting tools [5, 6]. Scheerlinck *et al* [7] printed an array of circular pillar structures of approximately 200–300 nm in diameter into a special photoresist using photolithographic equipment; however, their process required the manual removal of the imprint mold, utilized a photoresist not commonly used in tissue engineering applications, did not address critical issues such as mold and substrate surface treatment for optimizing pattern transfer, and did not address issues concerning the filling of features with critical dimensions down to around 50 nm where aspect ratios are usually very high. Moreover, torsional forces imparted by manually removing an imprint mold can severely damage nanoscale features patterned in brittle polymers like PEG-based hydrogels. Stuart *et al* [8] constructed modules out of 6061-T6 aluminum to outfit conventional mask aligners for automated UV-NIL; however, despite being useful add-ons to conventional mask aligners, their proprietary modules are quite complex. For the quick, reproducible and completely automated imprinting of nanoscale features into various homemade UV-curable materials, like PEG hydrogels, directly required by many research applications, dedicated nanoimprinting tools or proprietary add-ons to conventional mask aligners are not always necessary; this is especially the case in single-layer fabrication processes where alignment is not crucial.

PEG hydrogels like PEG-diacrylate (PEGDA) and PEG-dimethacrylate (PEGDMA) are polymers widely utilized as substrates in tissue scaffolds for cell-seeding applications. In particular, PEGDA and PEGDMA are ideal substrate materials for adipose and nervous tissue scaffolds used for adipose and nerve cell studies and tissue restoration for correcting deformities resulting from tumor resections, physical trauma, congenital abnormalities, aging and other medical conditions; they are non-allergenic, non-pyrogenic, look and feel natural, are stable after implantation or injection, and relatively inexpensive [9, 10]. A significant challenge in fabricating adipose and nervous tissue scaffolds in PEGDA and PEGDMA is having the ability to control the scaffold's physical topography at the nanoscale to closely resemble the topology of the extracellular matrix (ECM) of adipose and nerve cells.

In this work, we report a novel nanoimprinting method, called flash imprint lithography using a mask aligner (FILM), capable of imprinting nanoscale features—quickly, inexpensively and reproducibly—into UV-curable materials using a conventional optical mask aligner without any proprietary add-ons, expensive quartz templates, ad hoc material dispensers or dedicated imprinting tools, while still having the control, accuracy, reproducibility and complete automation of dedicated imprinting technologies. We demonstrate FILM by imprinting a portfolio of nanostructures in PEG-dimethacrylate (PEGDMA), a commonly used material in tissue scaffolds, down to a resolution of 50 nm using an optical aligner from SUSS Microtech (SUSS MA-6, SUSS Microtech, Munich, Germany).

2. Materials and methods

2.1. Synthesis of PEGDMA biomaterial

PEGDMA prepolymer of MW = 1000 (Polysciences Inc., Warrington, PA, USA, no. 25852-47-5) was dissolved in HPLC-grade demineralized water (Fisher Chemical, Fairlawn, NJ, USA, no. 7732-18-5) to a concentration of 100% (w/v). Irgacure 2959 photoinitiator (Ciba Specialty Chemicals, Tarrytown, NY, USA) was added to the PEGDMA/water mixture to a concentration of 0.1% (w/v) relative to the volume of water used (e.g. 0.001 g of Irgacure pure 1 mL of water). The PEGDMA was centrifuged for 30 min and refrigerated overnight to allow the mixture to stabilize.

2.2. Fabrication of silicon molds

Silicon wafers (NOVA Electronic Materials, Richardson, TX, USA) were diced into 20 mm × 20 mm pieces. The silicon pieces were ashed in an O_2-plasma asher (March CS-1701, March Plasma Systems, Concord, CA, USA) to burn off organic contaminants, cleaned in a mixture of 30% H_2O_2 (v/v) in H_2SO_4 (piranha solution) (hydrogen peroxide 30% no. 2190, sulfuric acid 96% no. 9684, J T Baker, Phillipsburg, NJ, USA) for 8 min and washed thoroughly in DI water. The wafer pieces were dried thoroughly with N_2 and then dehydration-baked at 200 °C for 5 min on a hot plate to remove all residual moisture. A 20 nm silicon dioxide layer was deposited on the clean silicon using plasma-enhanced chemical vapor deposition (PECVD) (Plasma-Therm 790, Plasma-Therm, Inc., St. Petersburg, FL, USA). ZEP-520A (Zeon Chemicals, Louisville, KY, USA) positive electronic resist was thinned in Anisole to a 1:3 ratio (v/v), respectively; ZEP-520A EBL resist was chosen due to its high resolution and dry-etch

resistance. The resist was deposited on the molds by spin-coating at 4000 rpm for 60 s to a thickness of approximately 100 nm and then soft-baked at 180 °C for 90 s. The resist was patterned using EBL (JEOL 6000 FSE, JEOL Ltd., Tokyo, Japan; Raith 50, Raith GmbH, Dortmund, Germany) and developed in ZED-N50 solution (Zeon Chemicals, Louisville, KY, USA). The patterned samples were descummed in an O_2 plasma to remove residual resist in the developed regions of the resist. Exposed silicon dioxide was etched through by RIE (Plasma-Therm 790, Plasma-Therm, Inc., St. Petersburg, FL, USA) using the resist as a mask. The resist was subsequently stripped in 30% H_2O_2 (v/v) in H_2SO_4. The exposed underlying silicon was etched with RIE using the patterned silicon dioxide layer as a mask. The silicon dioxide layer was then removed in buffered oxide etchant (BOE), leaving the patterned silicon.

2.3. Chemical pretreatment of silicon molds

Silicon molds were chemically treated with tridecafluoro-1,1,2,2-tetrahydrooctyl-1 trichlorosilane (United Chemical Technologies, Inc., Bristol, PA, USA, no. T2492). The silicon molds were ashed in an O_2-plasma asher to burn off organic contaminants and then immersed in a mixture of 30% H_2O_2 (v/v) in H_2SO_4 for 10 min, washed thoroughly in DI water, dried thoroughly with N_2 and dehydration-baked at 200 °C for 5 min on a hot plate. The clean silicon molds were then placed in a small container in juxtaposition to a small vial containing a few drops of the fluorinated-silane. The container was then covered and stored in a dehumidified nitrogen environment to prevent any reactions between the fluorinated-silane and ambient moisture. After 4 h, the silicon molds were removed and washed with a mixture of 25% carbon tetrachloride (v/v) in heptane and sequentially sonicated in acetone, methanol and isopropyl alcohol (IPA) (Acetone Certified ACS, Methanol Certified ACS, 2-Propanol Certified ACS, Fisher Chemical, Fairlawn, NJ, USA) for 5 min each. In between imprints using the mask aligner, residual photopolymerized PEGDMA was removed from the silicon molds by sequential immersion in acetone, methanol and IPA for 1 min each. After being chemically treated with the fluorinated-silane, the silicon molds were dried after each rinse with N_2 but never baked in an effort to preserve the silane layer.

2.4. Chemical pretreatment of glass microscope slides

Glass microscope slides were immersed in a mixture of 30% H_2O_2 (v/v) in H_2SO_4 for 10 min, washed thoroughly in DI water, dried thoroughly with N_2 and immersed in a 1 mM solution of 3-trichlorosilyl propyl methacrylate (TPM) in a mixture of 25% carbon tetrachloride (v/v) in heptane for 5 min. The piranha solution is a strong oxidizer that cleaned and hydroxylated the microscope slides; the silane attached to the hydroxyl groups (–OH) on the surface of the glass. Since TPM is highly reactive towards water, the microscope slides were meticulously dried before immersion in the silane solution. Because it was extremely difficult to remove all the residual moisture on the microscope slides using N_2 alone, the microscope slides typically formed a powdery-like surface when in contact with the silane solution. The powdery residue formed when the silane reacted with the residual moisture on the microscope slides that was not removed by the N_2. Moreover, unless the silane solution was kept in a dehumidified environment, moisture from the air often caused large particles to form in the silane solution that attached to the microscope slides. To limit the amount of powdery-like residue that formed and attached to the surface of the glass microscope slides, the silane mixture was stirred for the 5 min duration in which the microscope slides were immersed. Upon removing the microscope slides from the silane mixture, the silanized slides were copiously rinsed with a TPM-free mixture of 25% carbon tetrachloride (v/v) in heptane and then with 1X phosphate buffered saline (PBS). After rinsing, the microscope slides were dried with N_2 and stored in a vacuum desiccator. Carbon tetrachloride served to degrease superfluous silane that did not covalently bond to the silicon surface and remove particulate matter; excess silane was nearly impossible to remove with standard organic solvents like acetone, methanol and IPA. Pretreated glass slides were dried with N_2 after rinsing but were not dehydration-baked. Baking tended to degrade the tethered methacrylate groups on the glass slides, which reduced PEGDMA adhesion.

2.5. Examination of PEGDMA topography

Topological features imprinted in PEGDMA were examined using a field emission scanning electron microscope (FESEM) (LEO 1530, Carl Zeiss SMT Inc., Peabody, MA, USA) and atomic force microscope (AFM) (Dimension 3100 with Nanoscope IV controller, Digital Instruments & Veeco Metrology Group, Santa Barbara, CA, USA). AFM images were taken using a silicon tip in tapping mode (Tap300, Budget Sensors, Sophia, Bulgaria).

2.6. Examination of contact angles

Contact angle measurements were taken using a goniometer (FTÅ200, First Ten Angstroms, Inc., Portsmouth, VA, USA). Substrates were placed onto a manually adjustable sample stage and oriented appropriately; camera lighting, brightness and contrast were optimized. Small droplets of DI water were electronically dispensed onto the substrates using a syringe pump controlled by computer. Each image was taken a few seconds after a droplet was dispensed. Twelve data points were taken for each measurement to verify the accuracy and precision of contact angle data; measurements are reported as mean values with a corresponding standard deviation (SD). The baseline of the droplets was determined using a reflection image produced when the substrates were slightly tilted. The curvature of the droplets were traced using a non-spherical fit model. Information regarding contact angle measurements can be found in [11–15].

3. Results and discussion I: experimental details

3.1. Imprinting of nanostructures into UV-curable hydrogels

Details of the FILM process are illustrated in figure 1. Figure 2 shows images taken by a field emission scanning electron

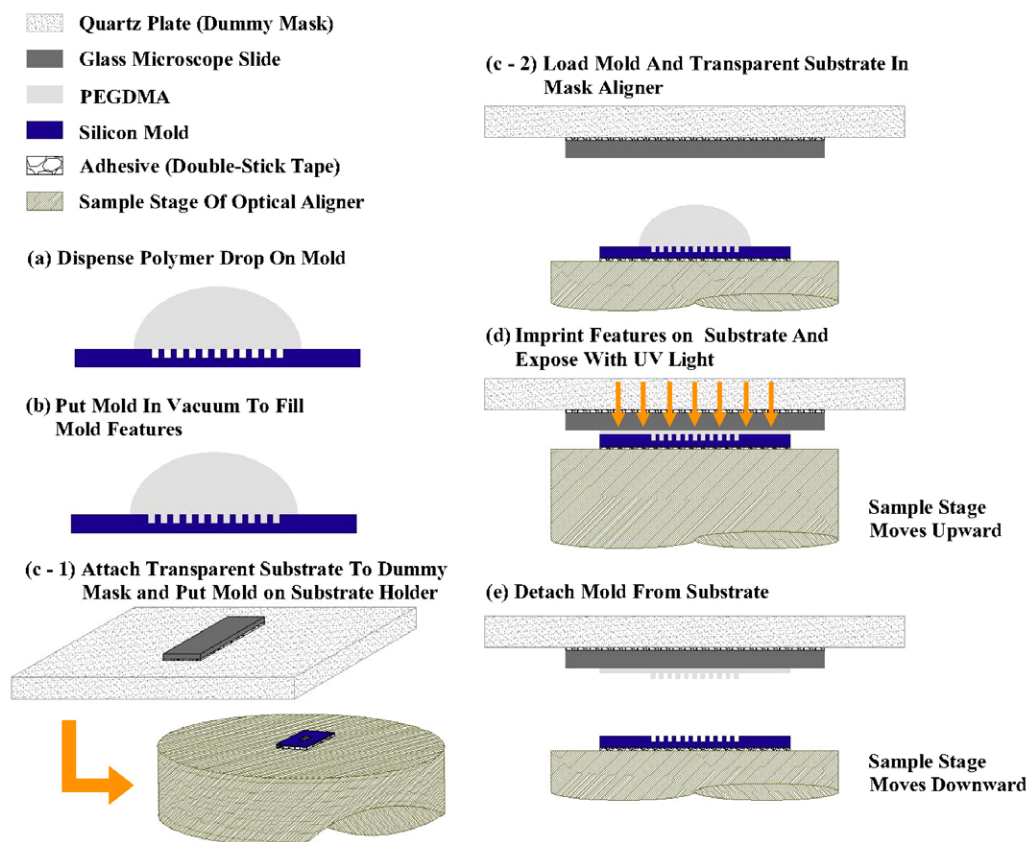

Figure 1. A schematic diagram of the FILM process used to imprint nanostructures from a silicon mold into UV-curable PEGDMA (other similar polymers can be utilized) using a conventional optical aligner commonly used in photolithography. (a) A drop of PEGDMA is deposited by pipette on a patterned silicon mold. (b) The mold with the drop is put in vacuum at room temperature and a pressure of 0.1 Torr for 10 min. ((c-1), (c-2)) The mold is positioned on the motorized sample stage of the optical aligner using an adhesive. A glass microscope slide is positioned on a quartz dummy plate using an adhesive (the dummy mask in (c-1) is inverted). The quartz plate adheres to a mask holder (not drawn) by suction and serves as a transparent dummy photolithographic mask. The mask holder snugly mounts into the optical aligner. The mold and glass slide can be aligned by eye with little difficulty. (d) The motorized sample stage ascends until the mold reaches the level of the glass slide while the mask holder assembly stays fixed; the final gap spacing between the mold and glass slide can be adjusted. The optical aligner's wedge-error compensation (WEC) feature wobbles the surfaces of the mold and glass slide until they are almost perfectly parallel for optimal pattern transfer. Exposure by UV occurs from the top through the quartz plate and glass slide (see orange arrows). Irradiation time can be set by the user and should be optimized for each particular UV-sensitive material. (e) The motorized sample stage detaches the mold from the slide by descending after exposure.

microscope (FESEM) of arrays of nanostructures of various geometries imprinted into PEGDMA. Figure 3 shows images taken by an atomic force microscope (AFM) illustrating the three-dimensional profiles of the nanostructures shown in figure 3.

3.1.1. Preparation step (figure 1(a)). UV-curable PEGDMA was synthesized by the procedure outlined in section 2. Silicon molds were fabricated using EBL and RIE; complete details of this procedure are also outlined in section 2. A 2 μl droplet of PEGDMA was deposited on the patterned area of a silicon mold by pipette. The volume of the droplet did not affect pattern transfer; however, droplets of superfluous size resulted in the formation of an excessive edge-bead around the edges of the imprinted region.

3.1.2. Vacuum step (figure 1(b)). The silicon mold with the dispensed droplet was put into a container with a flat surface in a vacuum desiccator at room temperature and a pressure of 0.1 Torr. The mold was typically kept under vacuum for 10 min. We found that putting the mold in vacuum was imperative for the consistent transfer of sub-micron patterns where aspect ratios were high; if the mold was not put in vacuum, then very inconsistent high aspect ratio pattern transfer was observed. When imprinting microscale features, where aspect ratios were low, the mold did not need to be put in vacuum. Keeping the mold under vacuum too long (>45 min) usually caused the PEGDMA droplet to completely evaporate. On the other hand, while a 10 min time period was most commonly used in our experiments, the time period could have probably been reduced further while yielding equivalent results (e.g. to around 5 min). Because the mold is treated to be very hydrophobic, surface tension forces do not naturally pull the interface into the features of the mold. The polymer is pushed into the features during the imprint step as pressure increases when the mold and glass slide are pressed together. We model polymer-filling behavior using finite element analysis; simulation results are presented in

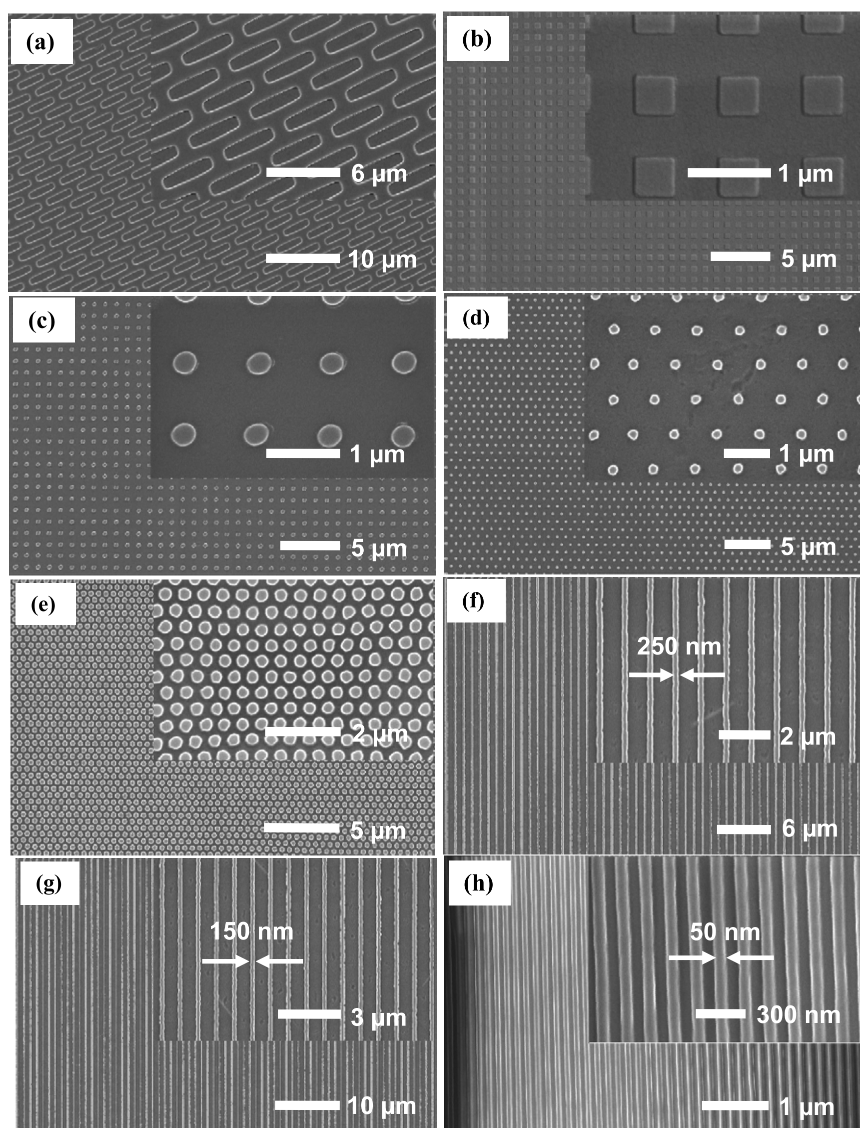

Figure 2. SEM images of various patterns imprinted from silicon molds into PEGDMA on glass microscope slides using the FILM process: (a) approximately 500 nm (short axis is a bit larger) by 4 μm (long axis) nanowells, (b)500 nm by 500 nm square pillars with a 1 μm pitch, (c) a square lattice of circular pillars of 300 nm diameter with a 1.3 μm pitch, (d) a hexagonal lattice of circular pillars of 150 nm diameter with a pitch of 1 μm, (e) a hexagonal lattice of circular pillars of 250 nm diameter with a pitch of 500 nm, (f), (g) lines of 250 nm and 150 nm width, respectively, with a pitch of 1 μm, and (h) lines of 50 nm width with a pitch of 150 nm. The pitch of the pillar structures is the same in both the horizontal and vertical directions.

section 4. The simulations elucidate the effects of nanofeature geometry on pattern transfer and establish the conditions when the vacuum step is necessary.

3.1.3. Silicon mold and glass slide alignment (figure 1(c-1), (c-2)). The features of the silicon mold were imprinted into the PEGDMA using a conventional optical mask aligner—the SUSS MA-6 (SUSS Microtech, Munich, Germany)—typically used for photolithography; in addition to using the MA-6 aligner, the FILM process can be adapted for use with almost any modern mask aligner since, aside from semantics, most aligner's function in the same manner. Using an adhesive, a chemically treated glass microscope slide was attached to a 5 inch by 5 inch square quartz plate, which was used as a dummy mask. The quartz plate was then attached to a mask holder by suction. The mask holder was inserted into the optical aligner and secured in place. As with the glass slide, a patterned silicon mold was attached with an adhesive to a substrate holder that fit onto the motorized stage of the optical aligner.

Conventional clear double-sided sticky tape worked well as an adhesive for both the glass slide and silicon mold. When the optical aligner is used for optical lithography, its normal mode of operation, an actual quartz-chrome mask is attached to the mask holder instead of the bare quartz plate that we utilized. The mask holder was a standard accessory for the optical aligner. No specially designed components were necessary. Most modern optical aligners use mask holders that support approximately 5 inch by 5 inch square quartz-chrome masks; however, as with the SUSS MA-6 and other modern optical

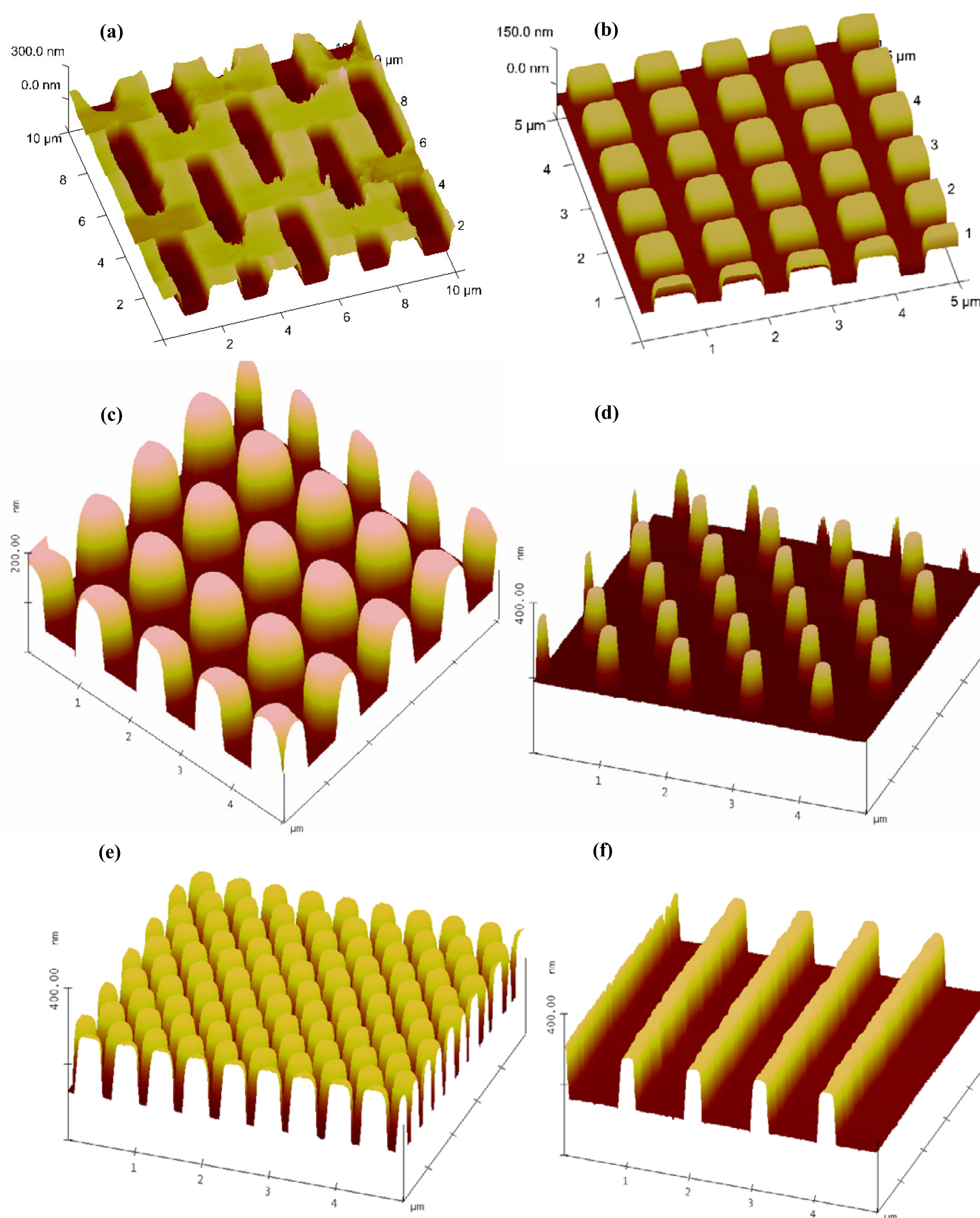

Figure 3. AFM images illustrating the three-dimensional topographies of the nanostructures shown in figure 2: (a) approximately 500 nm (short axis is a bit larger) by 4 μm (long axis) nanowells, (b) 500 nm by 500 nm square pillars with a 1 μm pitch, (c) a square lattice of circular pillars of 300 nm diameter with a 1.3 μm pitch, (d) a hexagonal lattice of circular pillars of 250 nm diameter with a pitch of 1 μm, (e) a hexagonal lattice of circular pillars of 250 nm diameter with a pitch of 500 nm, and (f) lines of 150 nm width with a pitch of 1 μm. Because the lines of 250 and 50 nm width have a nearly identical profile to that of the 150 nm lines, the AFM images of the 250 and 50 nm lines have not been included. All nanostructure arrays were imprinted in PEGDMA using the FILM process.

aligners, a myriad of mask holders that support different sizes of masks, are available. Any common mask holder can be used in the FILM process.

The motorized stage, where the silicon mold was attached, utilized a substrate holder that is also a common accessory for the mask aligner. Different substrate holders are available to support different sizes of substrates. The substrate holders normally use suction to attach glass or silicon wafers or other substrates in normal photolithography; however, since our silicon molds were small, an adhesive was required.

Alignment of the glass slide and mold was manually achieved by eye with little difficulty. Although most optical aligners contain microscopes, which allow for very tight control over alignment in multi-layer fabrication protocols, microscope precision is not typically necessary in single-layer processing.

3.1.4. Imprinting and exposure step (figure 1(d)). Once the mold and glass slide were positioned, the motorized stage of the optical aligner electronically elevated the silicon mold to

the level of the glass slide until reaching some explicitly set gap spacing; the gap spacing could be decreased until physical contact was made between the slide and mold or increased to very large spacings of greater than tens of microns. Whether the substrate holder is elevated to the level of the dummy quartz plate or the dummy quartz plate is lowered to the level of the substrate makes little difference in achieving pattern transfer. In the absence of the vacuum step, interfacial pressure forces build up and attempt to coerce the polymer into the nanofeatures of the mold as the mold and glass slide come together in imprinting. Simulation results provided by finite element analysis show a direct correlation between polymer-filling and the aspect ratio of the nanofeatures. Simulation results are presented in section 4.

After the mold was elevated to the glass slide, the PEGDMA was allowed to spread for about 30 s and then exposed with 365 nm *i*-line UV light with an intensity of approximately 12 mW cm^{-2}. The UV source of the optical aligner irradiated the PEGDMA from the top through the quartz plate and glass microscope slide for 45 s. Soft exposures were performed where a gap spacing was maintained during exposure; thus, the glass slide and mold were not directly in contact. Gap spacings of approximately 5 μm routinely achieved high-fidelity pattern transfer.

Figure 2 shows well-defined SEM images of arrays of nanostructures of various geometries imprinted into PEGDMA including (a) approximately 500 nm (short axis is a bit larger) by 4 μm (long axis) nanowells, (b) 500 nm by 500 nm square pillars with a 1 μm pitch, (c) a square lattice of circular pillars with a 300 nm diameter and pitch of 1.3 μm, (d) a hexagonal lattice of circular pillars with a 150 nm diameter and 1 μm pitch, (e) a hexagonal lattice of circular pillars with 250 nm diameter and 500 nm pitch, (f)–(g) lines of 250 nm and 150 nm width, respectively, with a pitch of 1 μm, and (h) lines of 50 nm width and a pitch of 150 nm. The pitch for the pillar arrays is equal in both the horizontal and vertical directions. As can be seen in figure 2, the imprint process reproducibly printed nanostructures with high fidelity over large areas. The thickness of the nanostructures was dependent on the thickness of the features in the silicon molds. Additionally, to facilitate good pattern transfer during imprinting, the silicon molds were etched so that the vertical wall profiles of the features in the mold sloped slightly inward. Thickness and vertical wall profile angle were controllable by varying parameters of the etch step during mold fabrication. When non-contact soft exposures were performed with user-defined gap spacings between the glass slides and silicon molds, the nanostructures were imprinted on a residual layer having a thickness equal to the gap spacing (with the exception of the 1 μm by 4 μm holes). Contact imprints, where the glass slide and silicon mold came into direct contact, could also be performed using the optical aligner. Contact imprints minimize the thickness of the residual layer. Because PEGDMA is a biocompatible material used in substrates for cell seeding, the residual layer is usually desirable. Figure 3 shows AFM images illustrating the three-dimensional profiles of the nanostructures shown in figure 2 including (a) the 500 nm $\times$ 4 μm nanowells, (b) the 500 nm $\times$ 500 nm square pillars, (c) the 300 nm circular pillars of 1.3 μm pitch, (d) the 150 nm circular pillars of 1 μm pitch, (e) the 250 nm circular pillars of 500 nm pitch, and (f) the 150 nm lines of 1 μm pitch. Because the vertical profiles of the 50, 150 and 250 nm line structures were almost identical, only the AFM image for the 150 nm has been included. The pillar structures in figures 3 (c)–(e) show that the FILM process can be used to imprint nanostructures of high density and aspect ratio. Structure depth can be altered by adjusting the duration for which the molds are etched.

The mask aligner allowed us to tightly control process variables that are important in imprinting high-fidelity nanometer-scale structures over large areas. First, by using the wedge-error compensation (WEC) function on the optical aligner, which is a feature typically found on most modern optical aligners in some form, the opposing surfaces of the glass slide and the silicon mold could be made to be almost perfectly parallel, which is necessary in achieving pattern transfer, imprinting nearly vertical structures, and in printing a patterned PEGDMA surface of constant thickness. Second, the optical aligner also allowed for a well-controlled exposure protocol. It was possible to perform a non-contact soft exposure at a user-defined gap spacing between the mold and glass slide during UV exposure. Additionally, the UV source used for polymerizing the PEGDMA produced intense, monochromatic and uniform UV radiation over the entire area of the pattern to be printed.

When utilizing opaque materials for the molds, like silicon, it is necessary to utilize a substrate transparent to UV in order to polymerize the UV-curable polymer. Since conventional glass microscope slides are commonly used transparent substrates for PEG-based scaffolds, we chose to utilize silicon molds due to the highly characterized properties of silicon with respect to micro-and nanoscale processing. If an opaque substrate is utilized, then the imprinting mold has to be transparent (e.g. quartz). Transparent molds have to be inserted into the aligner such that the UV radiation can pass through the mold to polymerize the UV-curable material on the opaque substrate; thus, the particular configuration is opposite to the one shown in figure 1(c). The transparent mold must be attached to the dummy quartz plate and the opaque substrate must be attached to the substrate holder from the bottom.

3.1.5. Mold detachment (figure 1(e)). After exposure, the motorized stage electronically separated the silicon mold from the glass slide. PEG hydrogels printed on unmodified glass do not adhere well during the separating step in the nanoimprinting process and subsequently in the presence of the aqueous buffer solutions used in cell culture. To facilitate adhesion of the PEGDMA to the glass slides, the slides were modified with surface-tethered methacrylate groups. Glass slides were treated with a methacrylated-silane, 3-trichlorosilyl propyl methacrylate (TPM); the acrylate groups of the silane covalently bonded to the PEGDMA upon polymerization to create an acrylate-activated glass surface. The silicon molds were treated with a fluorinated-silane, tridecafluoro-1,1,2,2-tetrahydrooctyl-1 trichlorosilane, to reduce adhesion to PEGDMA. The silane layer on the silicon molds remained intact for several tens of imprints. Details of the procedures

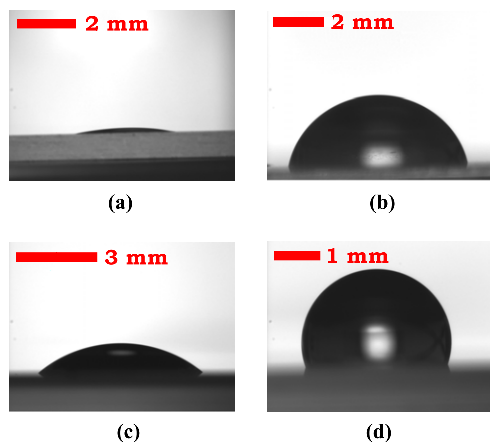

Figure 4. Contact angles of water in air on chemically treated and untreated glass microscope slides and silicon molds: (a) the contact angle of water on an untreated glass microscope slide. The contact angle is approximately 9.3° (SD = 3.2°). (b) The contact angle of water on a glass microscope slide treated with TPM. The contact angle is approximately 75.0° (SD = 6.5°). (c) The contact angle of water on the native oxide layer of untreated silicon. The contact angle is approximately 41.5° (SD = 7.7°). (d) The contact angle of water on silicon treated with a fluorinated-silane. The contact angle is approximately 104.2° (SD = 3.1°). In general, the mold and substrate must be chemically treated to optimize pattern transfer despite the choice of mold and substrate materials. Scale bars are based on the tilt angle of the stage (degrees) and base width (mm) of the drops.

used to treat the glass slides and silicon molds can be found in section 2. From a general perspective, it is important to note that the mold and substrate must be chemically treated to optimize pattern transfer, regardless of the choice of mold and substrate materials; adhesion of the UV-curable material to the mold must be reduced while adhesion to the substrate must be enhanced.

3.2. Contact angle measurements of water on chemically treated and untreated silicon molds and glass substrates

In order for sufficient pattern transfer to occur, silicon molds and glass substrates have to be chemically derivatized with various silanes (see sections 2.3, 2.4 and 3.1.5). To test the efficacy of our protocols used for treating the surfaces of the glass slides and silicon molds, contact angle measurements were taken using a goniometer; contact angles of water in air on glass and silicon are shown in figure 4. The contact angle on untreated glass microscope slides was approximately 9.3° (SD = 3.2°) (figure 4(a)). The untreated hydroxylated glass slides were extremely hydrophilic, having a contact angle of water in air approaching 0°. After silanizing, the contact angle on the glass slides increased to approximately 75.0° (SD = 6.5°) (figure 4(b)). The contact angle on untreated silicon with the silicon's native oxide layer was approximately 41.5° (SD = 7.7°) (figures 4(c)). After silanizing, the contact angle on the silicon increased to approximately 104.2° (SD = 3.1°) (figure 4(d)).

In their untreated states, the PEGDMA tended to stick to the glass slides rather than the silicon; however, if the glass slides were not treated with the acrylated-silane, delamination always occurred a few minutes after imprinting. Moreover, even when the glass slides were treated, adhesion between the PEGDMA and glass decreased significantly when the silicon mold was not treated. We believe that this resulted from the fact that greater tensile forces were required to detach the mold when the mold was not treated.

A significant advantage with using the optical aligner for imprinting was that it mechanically separated the mold from the glass slide without manual intervention. Detaching the mold by hand inevitably introduces torsional forces that can easily crack the silicon mold or destroy the nanostructures imprinted into the PEGDMA. Separating the silicon and glass manually should be avoided to achieve optimal pattern transfer and adhesion between the PEGDMA and glass slide.

4. Results and discussion II: simulations

4.1. Finite element modeling of polymer-filling into PEGDMA nanofeatures

Because surface effects are prominent at micron and sub-micron scales and the silicon mold was treated to be very hydrophobic, surface tension forces prevented the PEGDMA from naturally filling the nanofeatures. In the absence of the vacuum step, the imprinting step helped to push the polymer into the hydrophobic features of the molds. Whether polymer-filling occurred depended heavily on the aspect ratio of the nanofeatures. To study the relationship between aspect ratio and polymer-filling due to the imprinting step in the mask aligner, we conducted a finite element analysis using Comsol Multiphysics finite element software (Comsol Multiphysics Version 3.3, Comsol, Inc., Burlington, MA, USA).

In simulating the imprinting step, we consider the classical parallel-disc compression viscometer problem [16]. Figure 5(a) shows a schematic of a parallel-disc compression viscometer, which is analogous to the mold–substrate configuration in the mask aligner. Two circular discs of radius, R, which share a common axis of symmetry through their centers, are separated by a time-varying height, or gap spacing $H(t)$. The space between the plates is filled with an incompressible fluid of viscosity μ and density ρ. The upper circular disc moves at a velocity, v_0, towards the lower circular disc which is fixed in place. As $H(t)$ decreases, the fluid is 'squeezed', causing an axially symmetrical pressure drop and flow in the outwards radial direction. We can equivalently say that the bottom plate moves upward with velocity, v_0, towards a fixed upper plate, which is similar to the operation of the mask aligner where the mold (lower disc) is elevated at a prescribed velocity towards the fixed dummy plate supporting the glass slide (upper disc). Figure 5(b) shows the geometrical domain used in our nanofeature-filling simulations; the domain consists of an individual circular hole initially filled with air and a small region of fluid just above the hole. Two-dimensional axial symmetry has been utilized to reduce computing time; thus, figure 5(b) can be visualized as an extruded cylindrical solid formed by rotating the 2D geometry about the symmetry centerline axis. The height of the

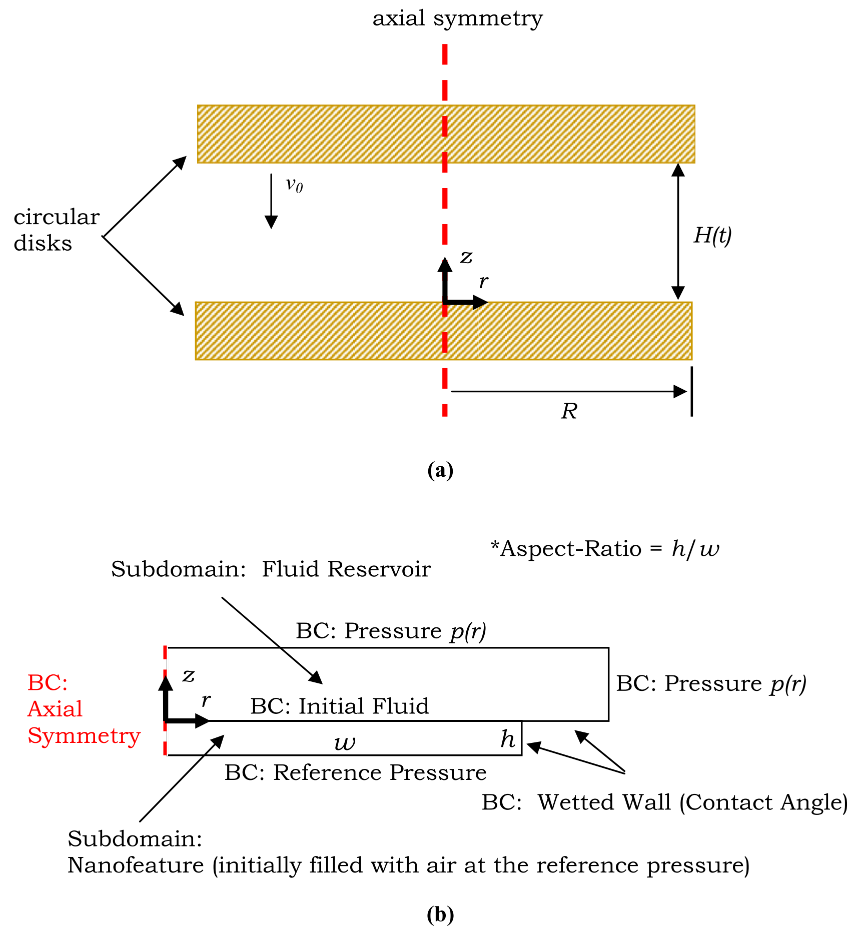

Figure 5. (a) A schematic diagram of the classical parallel-disc compression viscometer problem [16]. Two circular discs of radius, R, which share a common axis of symmetry through their centers, are separated by a time-varying height, $H(t)$. The space between the plates is filled with an incompressible fluid of viscosity μ and density ρ. The upper circular disc moves at a velocity, v_0, towards the lower circular disc which is fixed in place. As $H(t)$ decreases, the fluid is 'squeezed', causing a time-varying pressure drop in the radial direction. (b) A schematic diagram of the domain used in our transient nanofeature-filling simulations modeling the convection of polymer into the nanofeatures of the silicon mold. The domain utilizes axial symmetry; the 3D cylindrical domain can be visualized by rotating the 2D domain about the centerline symmetry axis. The domain consists of two subdomains, the fluid reservoir and the cylindrical nanofeature, which is initially filled with air. The boundary conditions utilized in our simulations are juxtaposed to their corresponding boundaries. The wetted-wall boundary condition applies a frictional force at the walls while simultaneously relating contact angle to surface tension. For high polymer-surface contact angles (i.e. for hydrophobic surfaces), surface tension forces restrict flow.

fluid region in figure 5(b) is small relative to the gap spacing between the mold and glass slide. Accordingly, the height of the fluid domain stays constant while the fluid's pressure increases as $H(t)$ decreases. The time-varying pressure distribution from the compression viscometer problem is used as a pressure boundary condition to simulate the effects of the change in $H(t)$.

The pressure of the air in the cylindrical hole is set at atmospheric pressure so that, neglecting gravitational effects, a balance between interfacial pressure, surface tension and frictional forces determines whether the hole is filled with the polymer. Because of the low molecular weight of our PEGDMA, which consists of water as its solvent, we model the liquid as being pure water. For higher molecular weight derivatives of PEG, non-Newtonian effects could come into play, and using a power law description of the polymer's viscosity may be more appropriate.

The polymer droplets dispensed onto the patterns of the silicon mold are typically large enough that the polymer spreads to fill the entire gap between the mold and glass slide almost instantly; consequently, we assume that the 'squeezing' of the polymer takes place when the gap between the mold and slide is completely filled with polymer in the derivation of the pressure boundary condition. At this point we also assume the following two things: the speed v_0 of the upper plate is slow such that a quasi-steady 'squeezing' process can be assumed and the initial starting height of the upper plate, H_0, is much less than the radius of the two discs, i.e. $H_0 \ll R$. In applying the conservation of mass, the rate of decrease in the volume of polymer between the discs must equal the rate of polymer outflow from the discs due to the 'squeezing' effect, i.e.

$$\pi R^2 v_0 = 2\pi R H(t) \langle v_r \rangle_{r=R} \quad \text{and}$$
$$\langle v_r \rangle_{r=R} = \frac{R}{2H(t)} v_0 \approx \frac{R}{H(t)} v_0 \tag{1}$$

where $\langle v_r \rangle_{r=R}$ is the radial velocity of the polymer at $r = R$. If the polymer velocity in the z direction, v_z, is assumed to be of the same order of magnitude as v_0 and the polymer velocity in the radial direction, v_r, is of the order of magnitude of $\langle v_r \rangle_{r=R}$, then $v_r \gg |v_z|$. The order of magnitude of the derivatives of the velocities can be estimated to be

$$\frac{\partial v_r}{\partial r} \approx \frac{(R/H(t))\, v_0 - 0}{R - 0} = \frac{v_0}{H(t)} \quad \text{and} \quad \frac{\partial v_z}{\partial z} \approx \frac{-v_0 - 0}{H(t) - 0} = -\frac{v_0}{H(t)}. \tag{2}$$

Neglecting the effects of gravity, the continuity and momentum equations simplify to

$$\frac{1}{r}\frac{\partial}{\partial r}(r v_r) + \frac{\partial v_z}{\partial z} = 0 \qquad \text{(continuity)} \tag{3}$$

$$-\frac{\mathrm{d}p}{\mathrm{d}r} + \mu \frac{\partial^2 v_r}{\partial z^2} = 0 \qquad \text{(momentum)} \tag{4}$$

with boundary conditions

BC1: $v_r = 0$; $v_z = 0$ at $z = 0$
BC2: $v_r = 0$; $v_z = -v_0$ at $z = H(t)$
BC3: $p = p_{\mathrm{atm}}$ (atmospheric pressure) at $r = R$ (free jet). (5)

From the governing equations (3) and (4) and boundary conditions, equation (5), the velocity distributions in the viscometer problem are

$$v_r = \frac{1}{2\mu}\left(\frac{\mathrm{d}p}{\mathrm{d}r}\right) z\,[z - H(t)] \quad \text{and} \quad v_z = \frac{1}{12\mu}\frac{1}{r}\frac{\mathrm{d}}{\mathrm{d}r}\left(r\frac{\mathrm{d}p}{\mathrm{d}r}\right). \tag{6}$$

Using the velocity distributions, the pressure distribution is derived to be

$$p - p_{\mathrm{atm}} = \frac{3\mu v_0 R^2}{[H(t)]^3}\left[1 - \left(\frac{r}{R}\right)^2\right]. \tag{7}$$

The pressure distribution is a function of radial position and the temporal height of the moving disk relative to the fixed disc, which we refer to as the gap spacing. Values for the radius of the discs, R, and the speed of the moving disc, v_0, are estimated based on our imprinting experiments with the mask aligner; thus, we estimate R based on the usual size of our silicon molds and v_0 by the speed at which either the silicon mold or glass slide moves (in the case of our experiments with the SUSS MA-6, the silicon mold moves upward to the level of the glass slide).

The polymer in the fluid reservoir is allowed to fill the cylindrical hole. Several forces affect whether the fluid will actually convect into the nanofeatures during the imprint step of the FILM process. Surface tension forces that naturally pull a fluid into small recesses with wetting surfaces, in our case, adversely restrict the flow of the polymer because of the high 104.2° (SD = 3.1°) contact angle between the polymer and the silicon surface. To complement the restricting surface tension force, frictional forces aid in retarding the fluid motion further. The counterbalancing force is the entrance pressure force that builds as the mold and substrate come together in the imprinting step, and is the result of the pressure drop across the convecting interface. The trapping of air is neglected, which is a mechanism of the assumption that the air is highly soluble in the polymer solution and simply diffuses out of the nanofeature as the polymer monomer enters; consequently, a constant pressure is maintained in the nanofeature as filling occurs. The no-gas-trapping assumption is consistent with Reddy *et al* [17], who modeled the flow of polymer in the S-FIL process. Assuming a constant air pressure in the nanofeature led us to define a constant pressure condition at the trough boundary in the nanofeature instead of a no-slip wall condition. If filling occurs, the pressure forces trap the polymer in the nanofeature for subsequent curing by UV. For the case of high aspect ratio features where feature-filling does not occur during the imprinting step, the vacuum step becomes necessary and imprinting and curing in the aligner should be done immediately following the removal of the mold from vacuum. We were unable to imprint high aspect ratio features even when incorporating the vacuum step if too much time elapsed between the vacuum step and the imprinting step. This could be attributable to the resistive surface tension forces coercing the polymer out of the nanofeatures.

The Navier–Stokes (NS) equation, equation (8), describes momentum transport for fluids. In considering the forces affecting the fluid bulk in our geometrical domain, a surface tension force, $\mathbf{F_s}$, is tagged onto the gravitational term on the right-hand side of the NS equation. To simplify our problem, gravitational forces are neglected, leaving only the surface tension force:

$$\rho\left(\frac{\partial \mathbf{v}}{\partial t} + \mathbf{v}\cdot\nabla\mathbf{v}\right) = \nabla p + \mu\nabla^2\mathbf{v} + \mathbf{f} \qquad \mathbf{f} = \rho\mathbf{g} + \mathbf{F_s} \approx \mathbf{F_s} \ \text{(gravity neglected)}. \tag{8}$$

The surface tension force acts at the polymer–air interface and is denoted as

$$\mathbf{F_s} = \nabla \cdot T \qquad T = \sigma\left[I - \left(\mathbf{n}\mathbf{n}^T\right)\right]\delta \tag{9}$$

where I is the identity matrix, $\mathbf{n}$ is the interface normal and δ is the Dirac delta function that equals 1 only at the air–polymer interface. A level-set two-phase computational technique is utilized in Comsol Multiphysics commercial finite element software to model the convection of the air–polymer interface [18]. The software sets up an equation in terms of a level-set function, ϕ, essentially defined as the proportion of polymer in a polymer–air mixture, that tracks the transport of the interface. The stochastic level-set function takes on only three values: $\phi = 1$ in polymer, $\phi = 0$ in air and $\phi = 0.5$ at the polymer–air interface. The level-set function is used to smooth the density and viscosity functions across the polymer–air interface.

As the silicon mold and glass microscope slide approach each other to a prescribed gap spacing, the polymer droplet

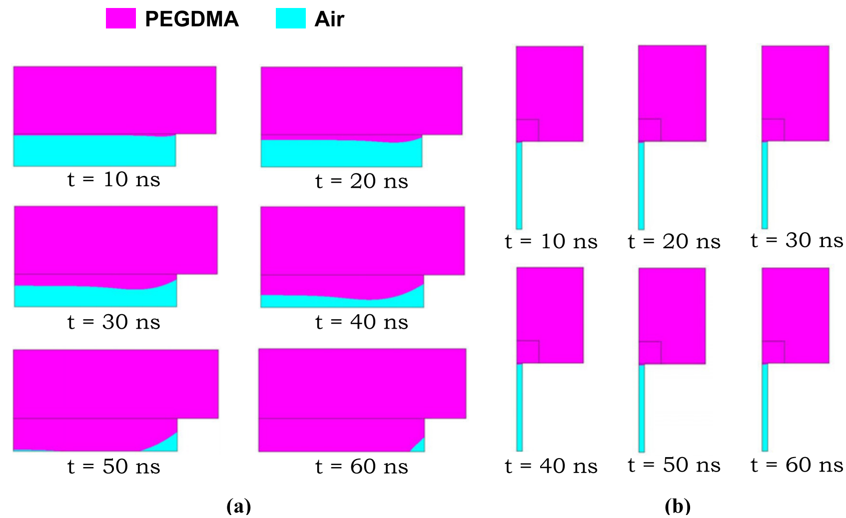

Figure 6. Simulated time-lapse images of the filling of cylindrical nanofeatures with a depth of 400 nm and an aspect ratio of (a) 1/10 and (b) 8 when $H_0 = 5\ \mu$m and $v_0 = 100\ \mu\text{m s}^{-1}$. The turquoise-colored areas represent air while the magenta-colored areas represent PEGDMA. Polymer filling occurs for the aspect ratio of 1/10 but does not occur for the aspect ratio of 8 (to re-emphasize, the nanofeatures in both (a) and (b) have a feature depth of 400 nm). Simulation results were obtained using Comsol Multiphysics commercial software.

spreads to fill the gap between the mold and slide. Polymer spreading occurs because of an asymmetrical pressure drop (equations (7)) about the concentric centerline axis of the two substrates. Because the initial pressure of the air in the nanofeature domain is at the reference pressure, the pressure drop across the interface coerces the fluid to enter the features of the mold. As stated earlier, surface tension forces, which are mathematically correlated to the contact angle of the polymer on the silicon, resist feature-filling due to the highly hydrophobic nature of the chemically treated silicon. Combined with a frictional boundary force exerted at the walls of the mold, $\mathbf{F_f}$ (equation (10)), instigated in our Comsol Multiphysics software, a balance of forces determines whether the nanofeatures of the mold fill with polymer:

$$\mathbf{F_f} = -\frac{\mu}{l}\mathbf{v}. \tag{10}$$

In equation (10), l is a characteristic slip length that we define to be of the order of the size of our finite elements near the nanofeature walls in our domain (figure 5(b)).

Figure 6 shows time-lapse images of our feature-filling finite element model applied to nanofeatures with an aspect ratio (height/width) of 1/10 and 8. The images plot the level-set function, which indicates either polymer or air. The magenta-colored areas represent polymer, where $\phi = 1$, while the turquoise-colored areas represent air, where $\phi = 0$.

As indicated by figure 6, filling occurs on the order of nanoseconds; thus, if we assume that the spacing between the silicon mold and glass slide is $H(t) = H_0 - v_0 t$, we can also assume that, for very small timescales, where $t \ll 1$ s, that $H(t) \approx H_0$.

By varying H_0 while holding the other parameters of equation (7) constant, including velocity, we can determine if filling will occur. It is important to note that, in many applications, it is desirable to have a thick residual layer and to actually delaminate the nanopatterned sheet of PEGDMA from the glass slide. To do this, the value of H_0 should be set much higher since it directly reflects the thickness of the residual layer. If the glass slide is not chemically treated with TPM, then the PEGDMA will delaminate as a nanopatterned sheet a few minutes after exposure.

Figure 7 shows the relationship of H_0 versus aspect ratio when feature-filling occurs in the nanofeatures. Consistent with our experiments, you can see in figure 6 that, as aspect ratio increases, the required gap spacing for imprinting decreases; moreover, the gap spacing at which feature-filling occurs decreases with power regression behavior as aspect ratio increases. The power regression curve was generated in Matlab using the least squares curve-fitting technique; in our case, a linear curve was fitted to the logarithm of the aspect ratio and height-of-filling data to find the constants, a_k, in the general power law form, $y = a_0 x^{a_1}$.

As the gap spacing decreases, the pressure drop across the polymer–air interface increases, providing a greater push for filling to occur. The gap spacing in the aligner we utilized (SUSS MA-6), could be changed in 1 μm increments; thus, the lowest gap spacing we could exhibit in our experiments was 1 μm. From our observations, even with a 1 μm setting, the need for the vacuum step (figure 1(b)) became necessary for consistently printing structures with aspect ratios > 1; without the vacuum step, printing high aspect ratio structures either did not occur on a consistent basis or did not transfer well over large areas. We believe that trapped air in the features of the mold is released when the silicon mold is put in a low-pressure environment; accordingly, the capillary pressure is somehow overcompensated by mechanical pressure driving the polymer into the feature.

4.2. Verification of finite element modeling methodology

We verify our level-set simulation methodology in Comsol Multiphysics by comparing results obtained for the surface-tension-driven convection of a blood–air interface in a narrow

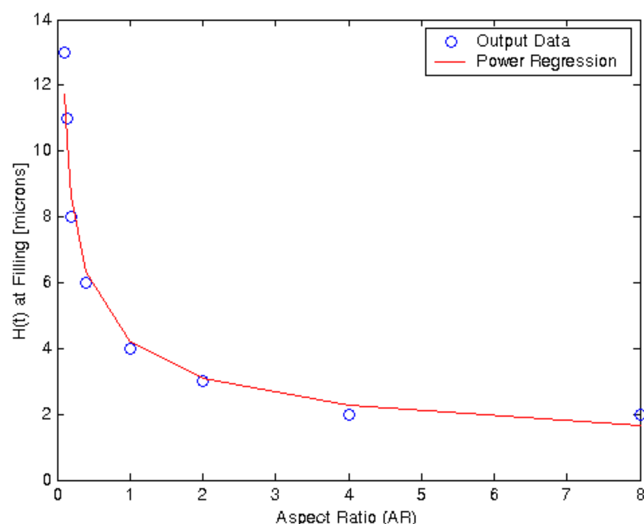

Figure 7. A plot of the gap spacing at which nanofeature-filling occurs versus aspect ratio (AR $= h/w$). For increasing aspect ratios, the required gap spacing for filling decreases. Nanofeature-filling behavior follows power regression behavior according to the equation listed in the plot.

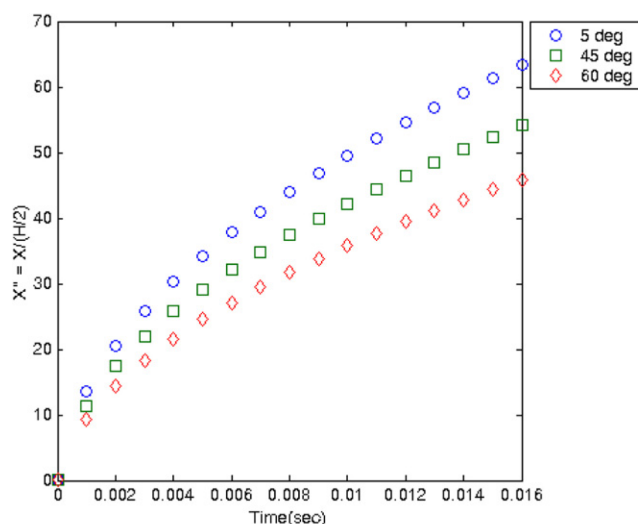

Figure 8. The non-dimensional position of a blood–air interface as a function of time and contact angle in a horizontal rectangular slit predicted by our level-set methodology in Comsol Multiphysics. Our results agree closely with those presented by Huang *et al* [19]. The height H of the slit is 0.05 mm. Non-dimensional position X'' is given by $X'' = X/(H/2)$, where X is position in meters. The chart closely approximates the simulated behavior in figure 12 of [19].

rectangular slit at various contact angles with those obtained by Huang *et al* [19]. Figure 8 shows plots of the dimensionless position of the blood–air interface as a function of time for the first 0.016 s. Our results agree closely with those of figure 12 in [19].

One thing to note is that we utilize the NS equations to model the physics because we simulated the flow of liquid water. As the size of the nanofeatures reduce to a few nanometers, molecular dynamics (MD) models may be more appropriate. Because we model solely the flow of liquid water, which consists of very tightly packed water molecules, we deemed the NS equations appropriate for our purposes.

5. Conclusions

We have demonstrated an automated nanoimprinting method, flash imprint lithography using a mask aligner, termed FILM, for transferring nanoscale features from silicon molds into widely utilized photopolymerizable PEG hydrogels on glass microscope slides using a conventional optical mask aligner. We were able to fabricate nanoscale structures in PEGDMA down to 50 nm without the use of expensive dedicated nanoimprinting tools, quartz templates and material dispensers, and without any manual intervention.

Mask aligners allow control over many process variables that are important in reproducibly imprinting high-fidelity nanometer-scale structures over large areas. Although we specifically utilized a SUSS MA-6 optical aligner, the FILM process can be adapted for use with many other modern optical aligners since they generally function in the same manner. Additionally, the FILM process can be used to pattern nanostructures in other low-viscosity UV-curable polymers alongside PEG hydrogels without the use of ad hoc material dispensers often required with dedicated nanoimprinting tools. We were also able to utilize cheap silicon molds instead of expensive quartz templates, required by some imprint tools (e.g. S-FIL), which allowed us to imprint various topographies at very little cost. Moreover, molds of many different materials can be used provided that either the mold or substrate material is transparent to UV. We believe that the generalized FILM process is very well suited for creating various physical topographies in UV-curable materials like PEG hydrogels for fabricating biomimetic tissue scaffolds used in cell-seeding applications. We are currently working on imprinting sub-50 nm features and using the FILM process to study the effects of physical nanotopography on the adhesion, migration and differentiation of preadipocytes (fat cell precursors) found in adipose tissues and on axon polarization of hippocampal cells; thus far, the FILM process has vastly improved our ability to do high-throughput studies, which is very important in creating new therapies for adipose and nervous tissue damage.

Acknowledgments

This work was supported by research grants from the National Science Foundation (NSF) and Office of Naval Research. Work was performed in part at the Center for Nano and Molecular Science and Technology (CNM) and at the Microelectronics Research Center (MRC), a part of the National Nanofabrication Infrastructure Network supported by NSF (award no. 0335765) at UT-Austin.

References

[1] Revzin A, Russell R J, Yadavalli V K, Koh W G, Deister C, Hile D D, Mellott M B and Pishko M V 2001 *Langmuir* **17** 5440–7
[2] Hahn M S, Taite L J, Moon J J, Rowland M C, Ruffino K A and West J L 2006 *Biomaterials* **27** 2519–24
[3] Chou S Y, Krauss P R and Renstrom P J 1995 *Appl. Phys. Lett.* **67** 3114–6

[4] Colburn M *et al* 1999 Step and flash imprint lithography: a new approach to high-resolution patterning *Proc. SPIE's 24th Int. Symp. on Microlithography: Emerging Lithographic Technologies III (Santa Clara, CA, March 1999)* vol 3676, pp 379–89, Part One

[5] Kim P, Kim D H, Kim B, Choi S K, Lee S H, Khademhosseini A, Langer R and Suh K Y 2005 *Nanotechnology* **16** 2420–6

[6] Jung G Y, Ganapathiappan S, Ohlberg D A A, Olynick D L, Chen Y, Tong W M and Williams R S 2004 *Nano Lett.* **4** 1225–9

[7] Scheerlinck S, Thourhout D V and Baets R 2005 Nano imprint lithography for photonic structure patterning *Proc. Symp. IEEE/LEOS Benelux Chapter (Belgium)* pp 63–6

[8] Stuart C, Xu Q, Tseng R J, Yang Y, Hahn H T, Chen Y, Wu W and Williams R S 2006 *J. Vac. Sci. Technol.* B **24** 539–42

[9] Patel P N, Smith C K and Patrick C W 2005 *J. Biomed. Mater. Res.* A **73** 313–9

[10] Lu Y, Mapili G, Suhali G, Chen S C and Roy K 2006 *J. Biomed. Mater. Res.* A **77** 396–405

[11] Adamson A W 1982 *Physical Chemistry of Surfaces* (New York: Wiley)

[12] Andreas J M, Hauser E A and Tucker W B 1938 *J. Phys. Chem.* **42** 1001–19

[13] Adamson A W, Shirley F P and Kunichika K T 1970 *J. Colloid Interface Sci.* **34** 461–8

[14] Fowkes F M and Harkins W D 1940 *J. Am. Chem. Soc.* **62** 3377–86

[15] Girifalco L A and Good R J 1957 *J. Phys. Chem.* **61** 904–9

[16] Bird B R, Stewart W E and Lightfoot E N 2002 *Transport Phenomena* (New York: Wiley)

[17] Reddy S and Bonnecaze R T 2005 *Microelectron. Eng.* **82** 60–70

[18] Sussman M, Fatemi E, Smereka P and Osher S 1998 *Comput. Fluids* **27** 663–80

[19] Huang W, Bhullar R S and Fung Y C 2001 *J. Biomech. Eng.-Trans. ASME* **123** 446–54